# Transmission Electron Microscopy of Actinide Materials

Kevin Moore, Mark Wall, Adam Schwartz
Lawrence Livermore National Laboratory

This work was performed under the auspices of the U.S. DOE by LLNL under contract W-7405-Eng-48



# Introduction

Actinide metallurgy, crystallography, physics, and chemistry are of great interest due to the unique behavior of the 5*f* states that dominate the electronic structure.

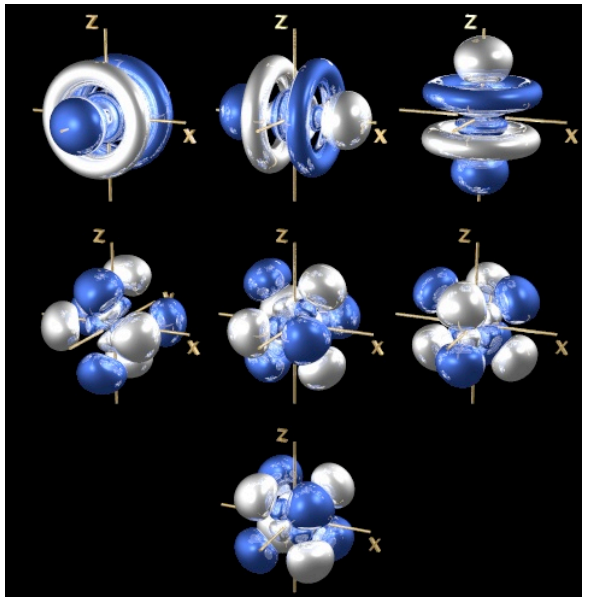


The 5*f* states produce a wide range of fascinating behaviors in the actinide materials. from superconductivity to exotic magnetism.

Accordingly, they are of great interest, but are difficult to work with.

Transmission electron microscopy (TEM) can overcome many of the problems of working with actinide materials and can be used to interrogate the atomic and electronic structure of actinide materials.

We will cover our capabilities at LLNL:

* Sample preparation
* TEM techniques
* *in situ* capabilities

# Sample preparation

An important part of actinide research is safe handling and sample preparation.

We have a complete in-house suite for TEM sample preparation:

- 2 inert gas glove boxes
- Ability to shape and anneal samples
- Electropolishing equipment and precision ion mill
- Vacuum-transfer TEM holders for heating and cooling

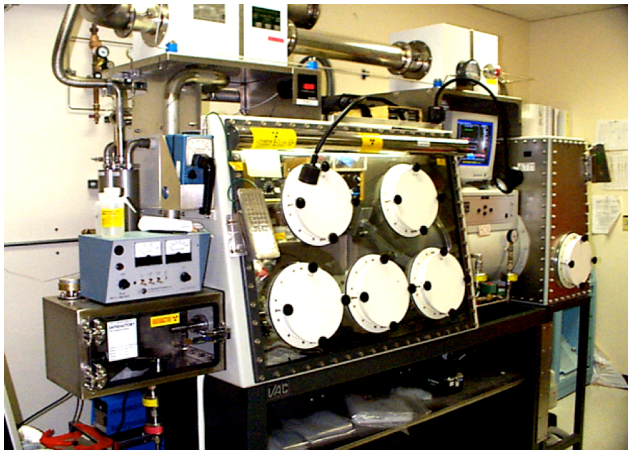

Vacuum transfer

to TEM for analysis

# Transmission electron microscopy

## ATOMIC STRUCTRE

Imaging:

- Bright- and dark-field imaging
- High resolution TEM (HRTEM)

Diffraction:

- Parallel illumination
- Convergent-beam electron diffraction (CBED)
- Scanning TEM (STEM / *Z* contrast)

## CHEMISTRY

Spectroscopy:

- Energy dispersive x-ray spectroscopy (EDXS)

## ELECTRONIC STRUCTURE + CHEMISTRY

Spectroscopy:

- Electron energy-loss spectroscopy (EELS)

# Bright- and dark-field imaging

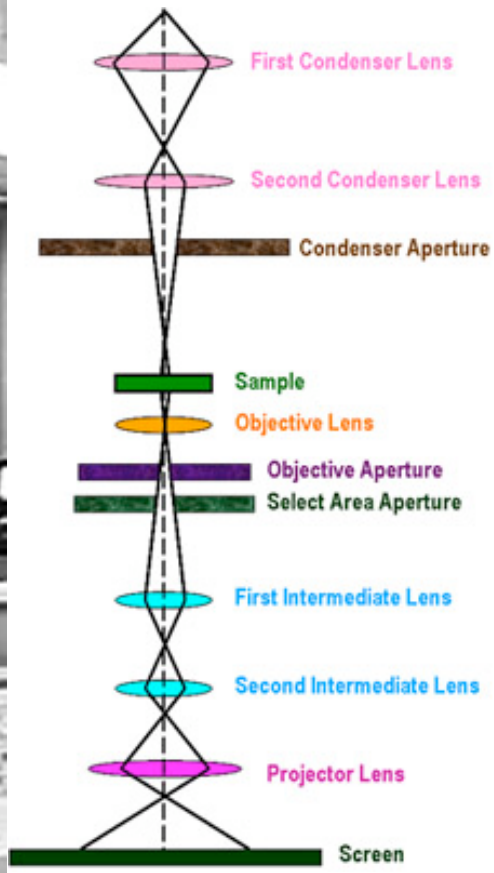


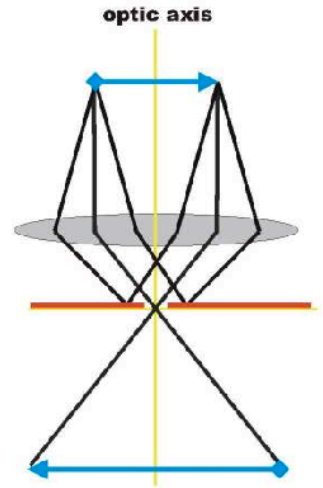


**Bright-field**: forming an image using the 000 beam.

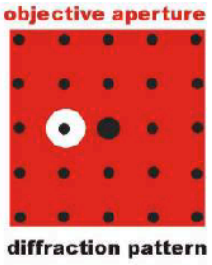


**Dark-field**: Using only specific higher-order reflection; excluding 000 beam.

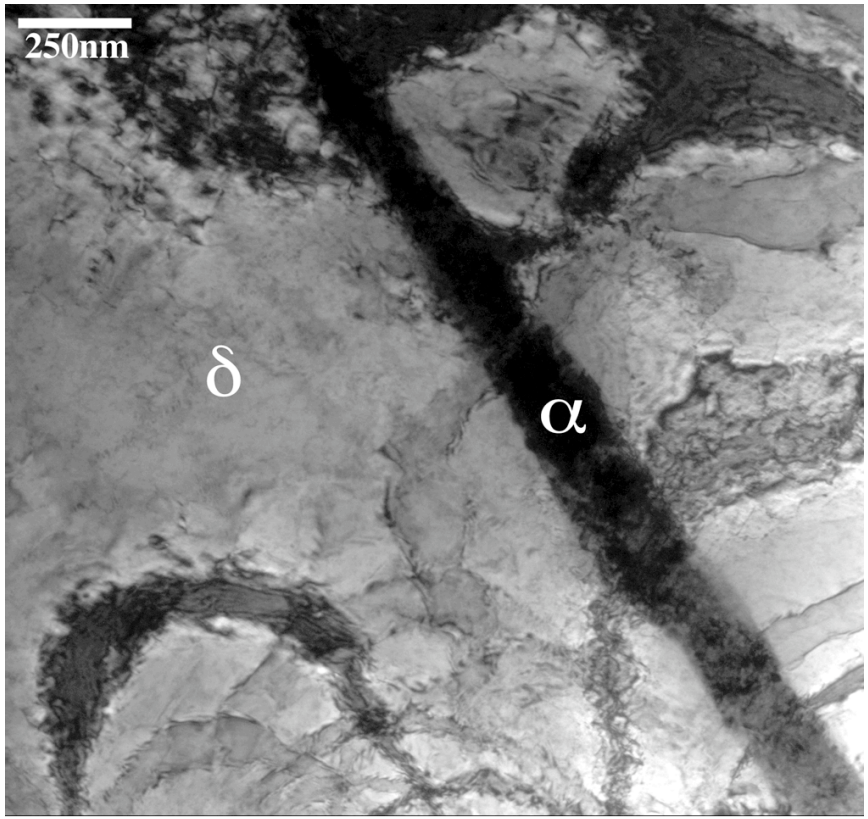


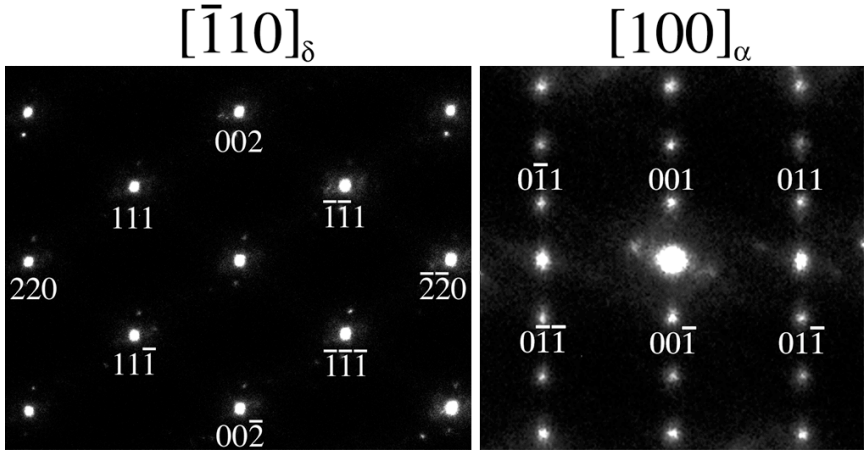


Moore *et al.*, *Phys. Rev. Lett.* 2003.

## Bright-field imaging of an α′ + δ two-phase mixture in Pu-Ga

Isothermal martensitic transformation:

α' plate in a δ matrix that has been formed by cooling the sample to -120°C for 10 hours.

The orientation relationship between α' and δ is:

$(111)_\delta \parallel (020)_{\alpha'}$

$[110]_\delta \parallel [100]_{\alpha'}$

as shown Previously by Zocco *et al.* Acta Met. 38 (1990).

# Bright field images of dislocation densities around α′ plates in Pu-Ga alloys

Dislocation density is 6-7 times greater near α′/δ interfaces.
Plasticity relieves large dilational strains near tips of α′ plates.
Compare to elastic-plastic FE calculations.

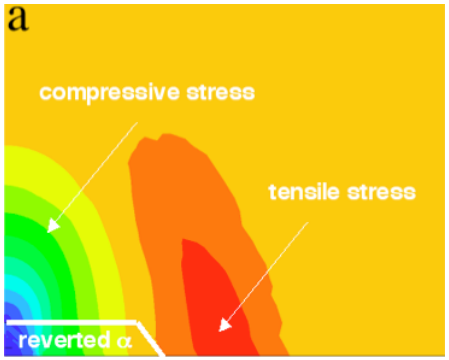


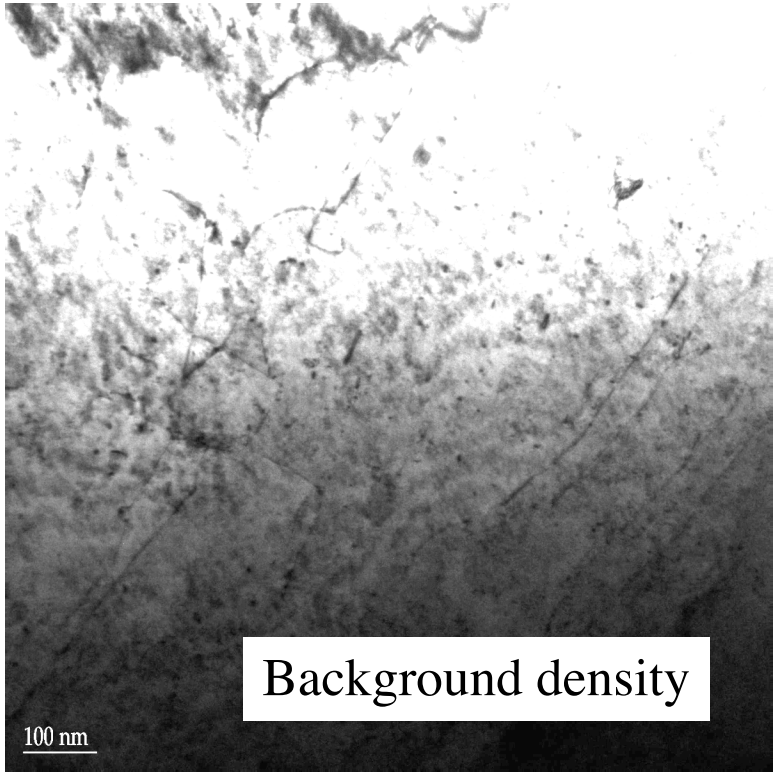


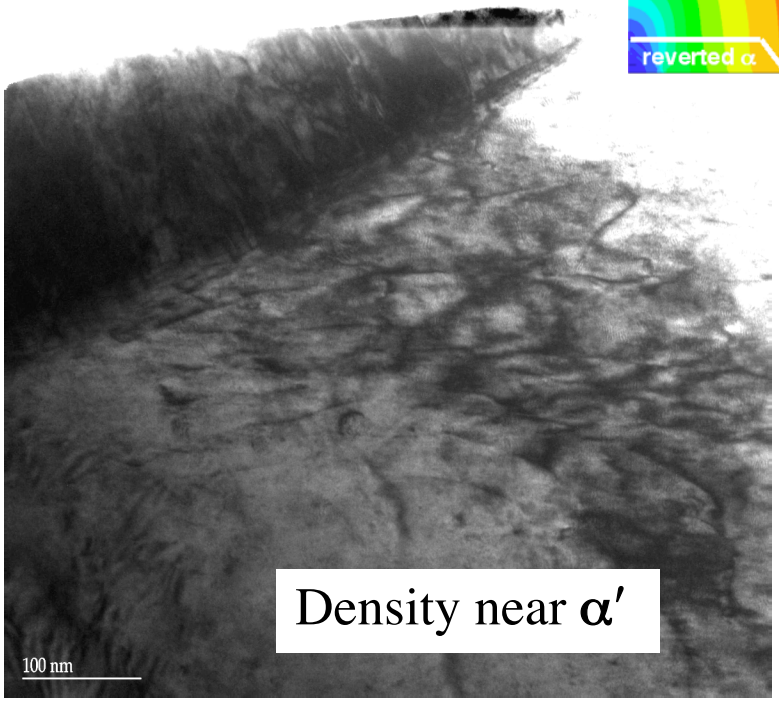


Krenn *et al. MRS Proc.* 2004.

# Bright-field imaging of twins in α′

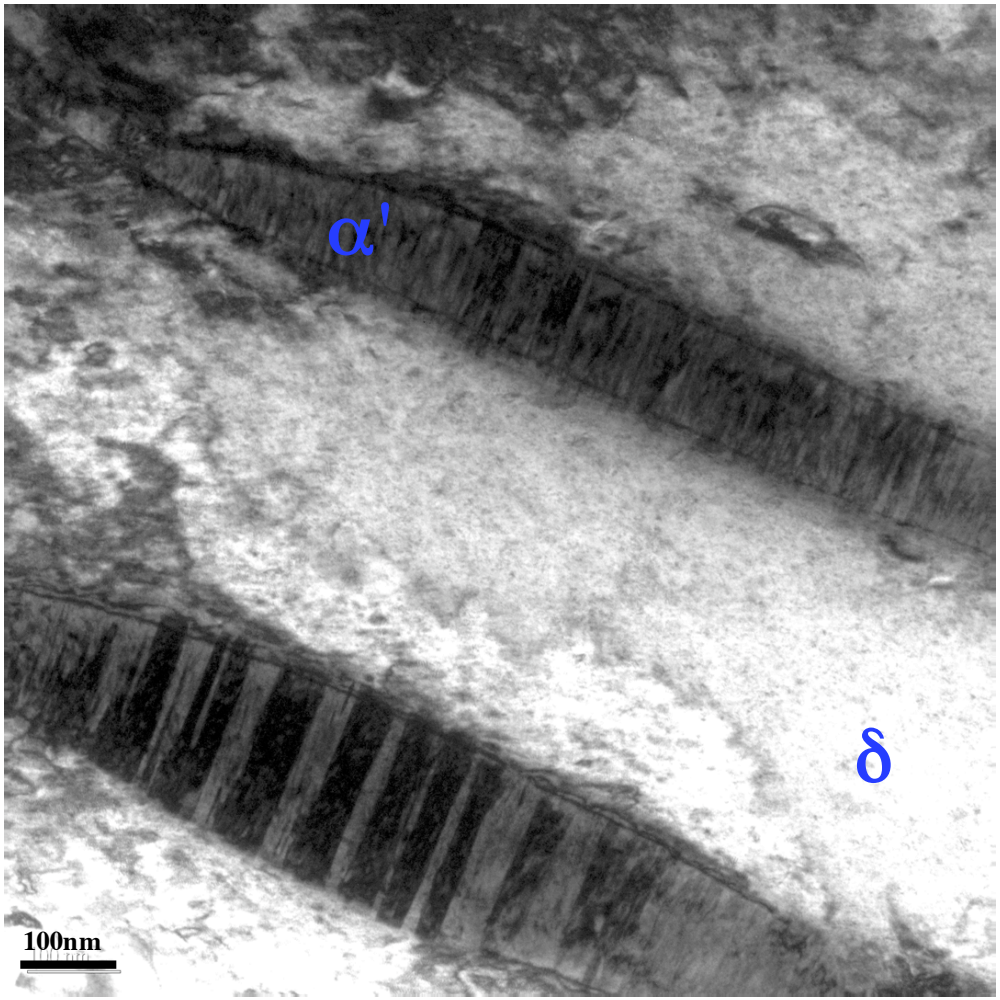


α′ plates usually contain numerous twins as shown in the TEM image left.

TEM reveals (205)α' twinning as a lattice invariant deformation mode.

These can also be examined in dark-field using specific reflections…

# Dark-field TEM imaging of twins in α′

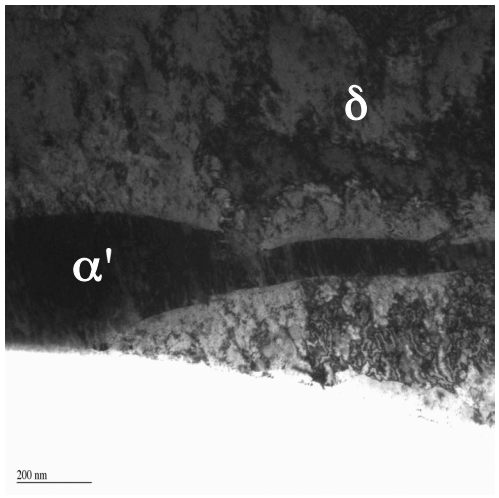


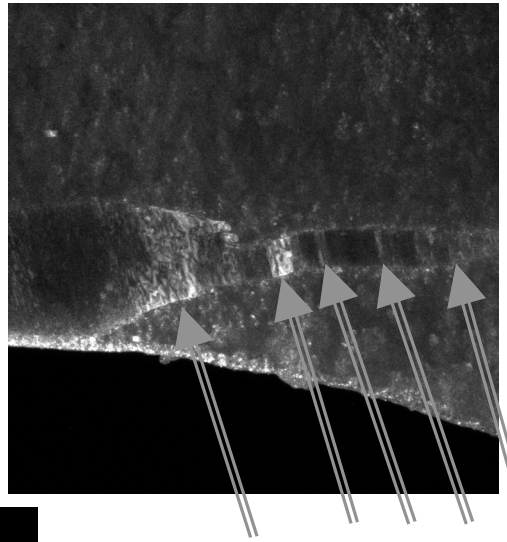

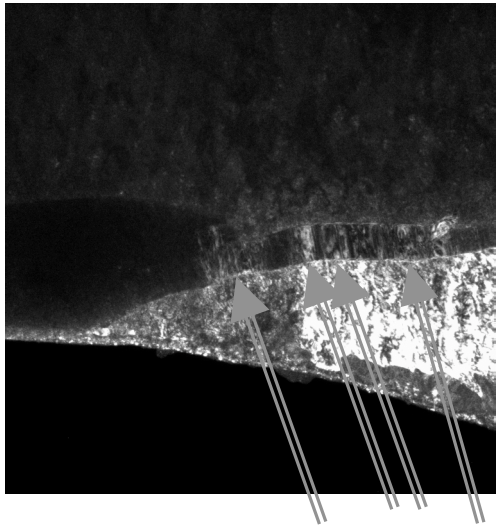

$[020]_{\alpha'}$
$[111]_{\delta}$

Bright #1 variant

Bright #2 variant

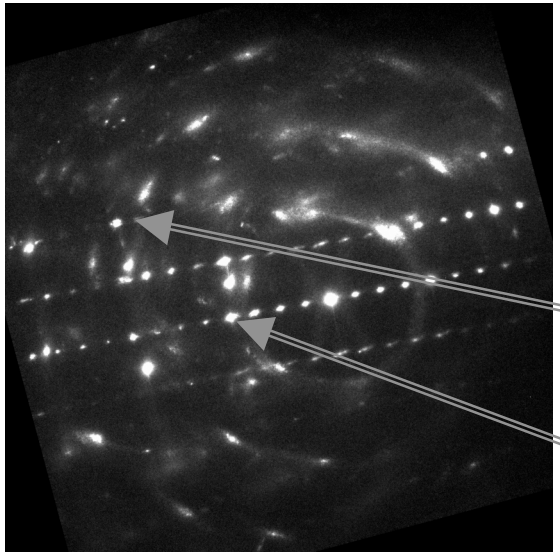

Diffraction spot from Variant #2

Diffraction spot from Variant #1

Two variants share a common $[020]_{\alpha}$ direction, but differ by a 60 degree rotation about $[020]_{\alpha}$.

Interfacial plane is ∥ $(110)_{\delta}$.

# Experimental and simulated electron diffraction of twins in α′

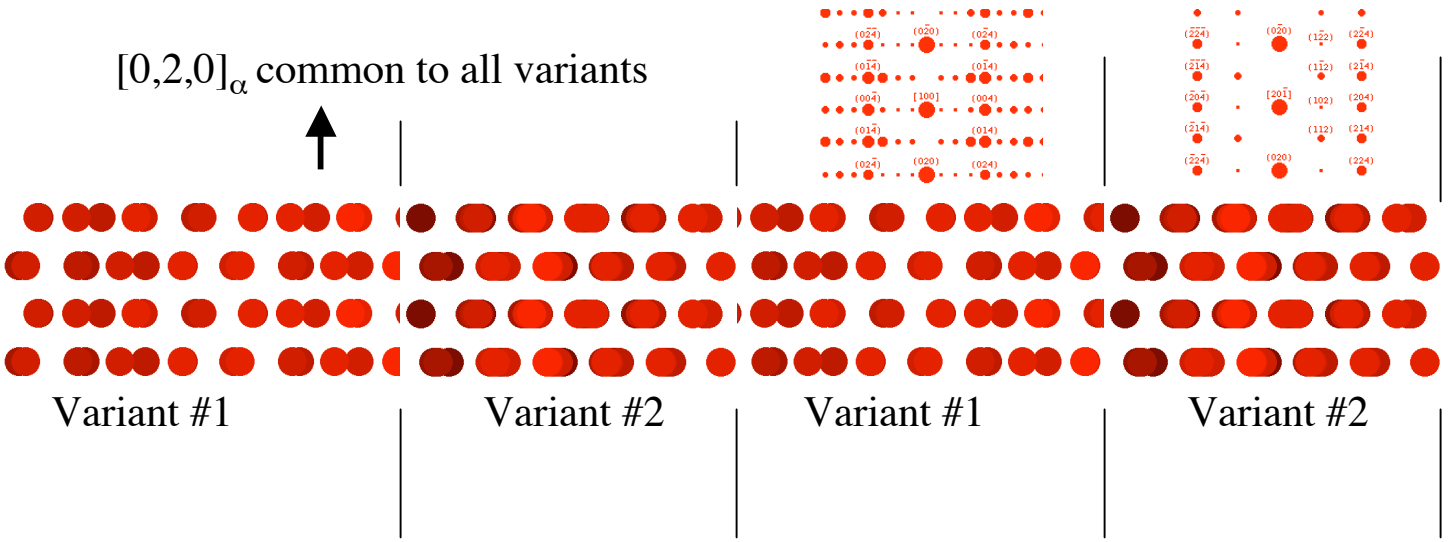


Calculated SAD of $[-1,1,0]_\delta$

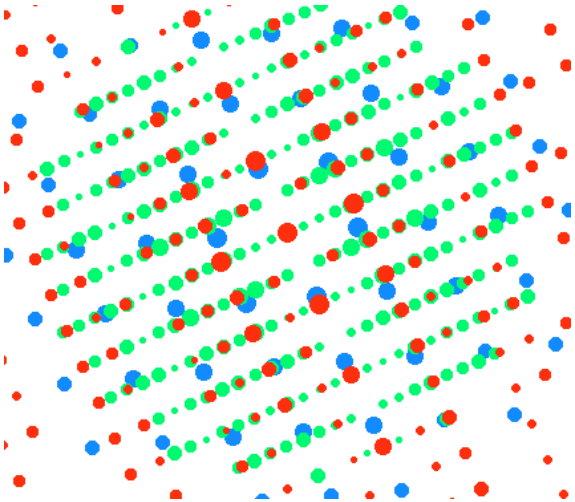

Acquired SAD of $[-1,1,0]_\delta$

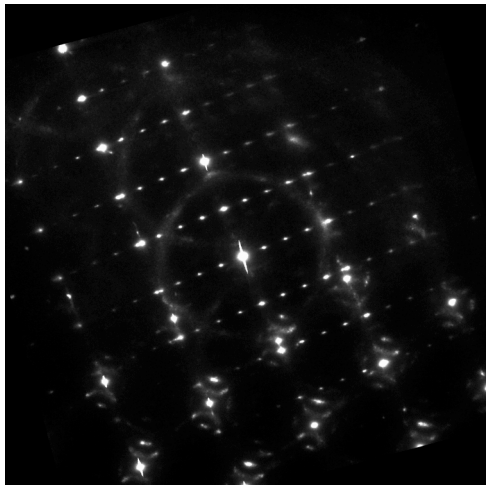

**Two variants share a common $[020]_\alpha$ direction, but differ by a 60 degree rotation about $[020]_\alpha$**

# High resolution TEM imaging

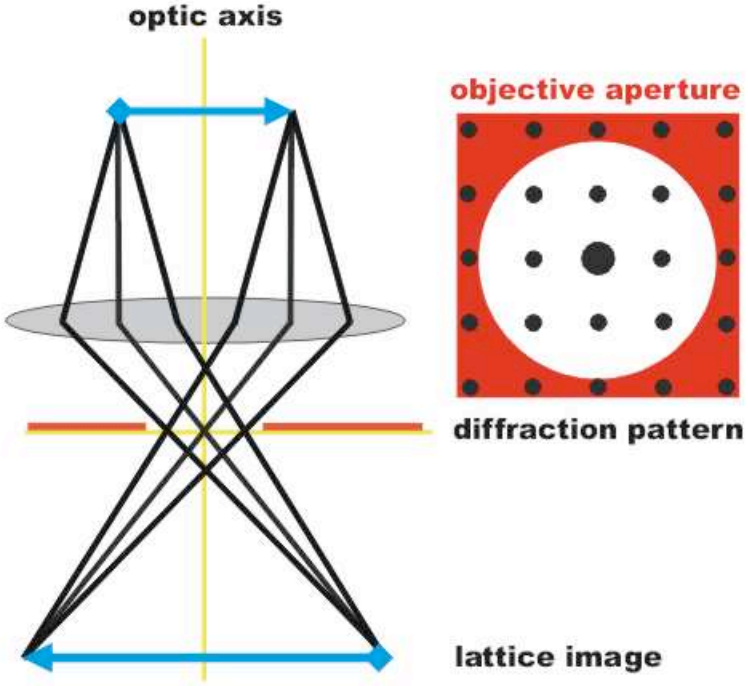


In the case of HRTEM the images are formed using numerous Bragg reflections.

Bloch waves interact with the sample differently on and off columns of atoms.

This produces phases interactions between the beams, and in turn *phases contrast* in the HRTEM image.

# High resolution TEM imaging of δ Pu

HRTEM image of δ-Pu viewing along the (100) zone axis.

The image shows the repeat of the atomic structure and the axis of 4-fold symmetry.

Otherwise, it is rather boring.

We can use this technique to look at more exciting and scientifically meaningful things…

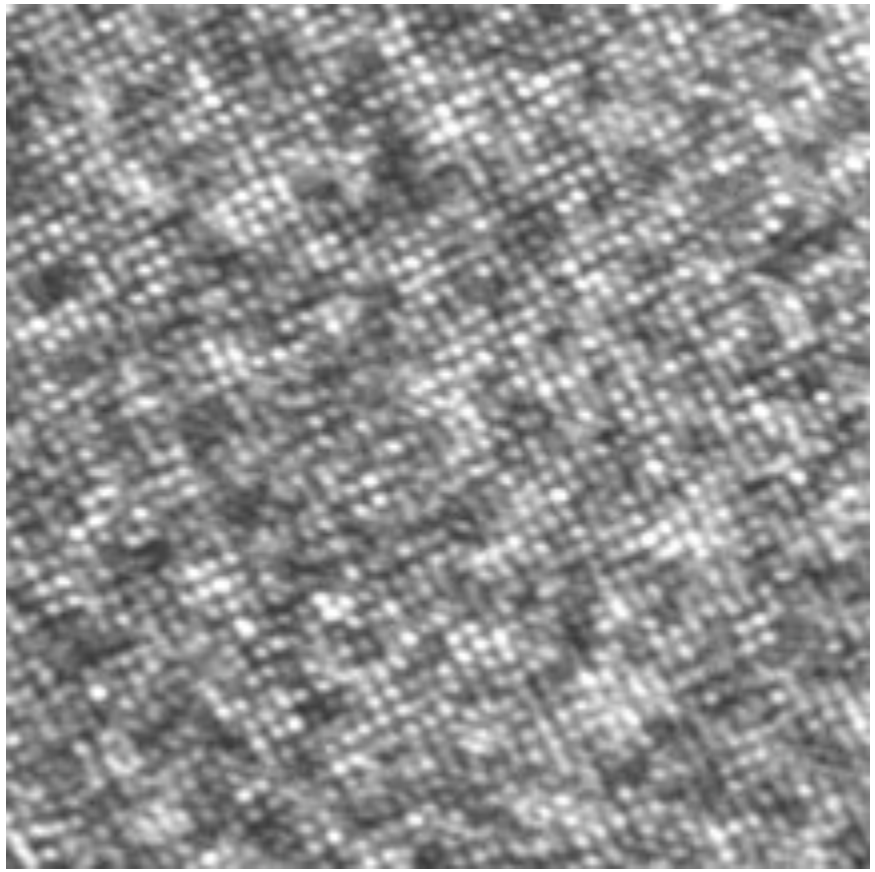

# High resolution TEM imaging of the α′/δ interface

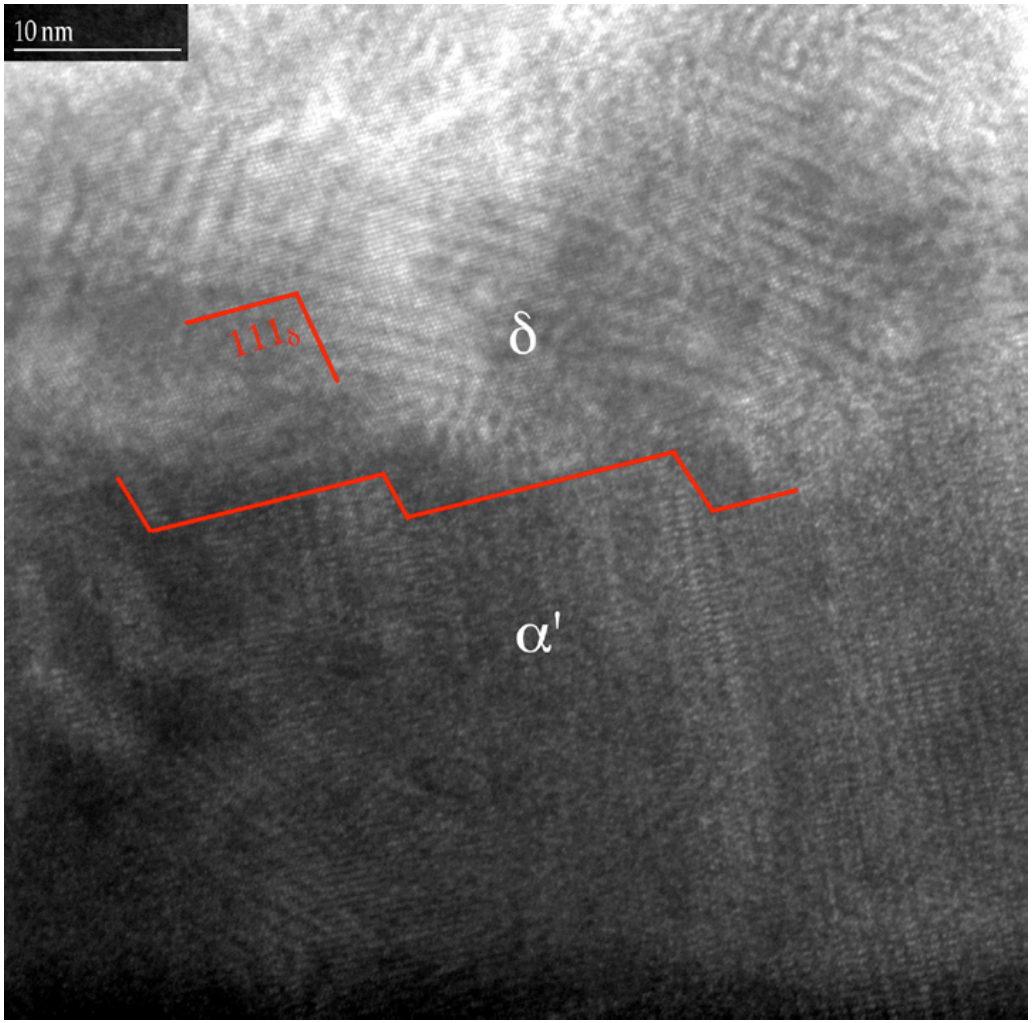


Moore *et al.* Philosophical Magazine (in review).

One pressing question: what is the orientation of the α′ habit plane in the δ matrix?

HRTEM images shown that the α′/δ interface is composed of a terrace and ledge structure that is faceted on $111_\delta$.

This means that the ***macroscopic*** interface and interfacial curvature is facilitated by the number and density of ledges on the interface.

# Scanning transmission electron microscopy (STEM)

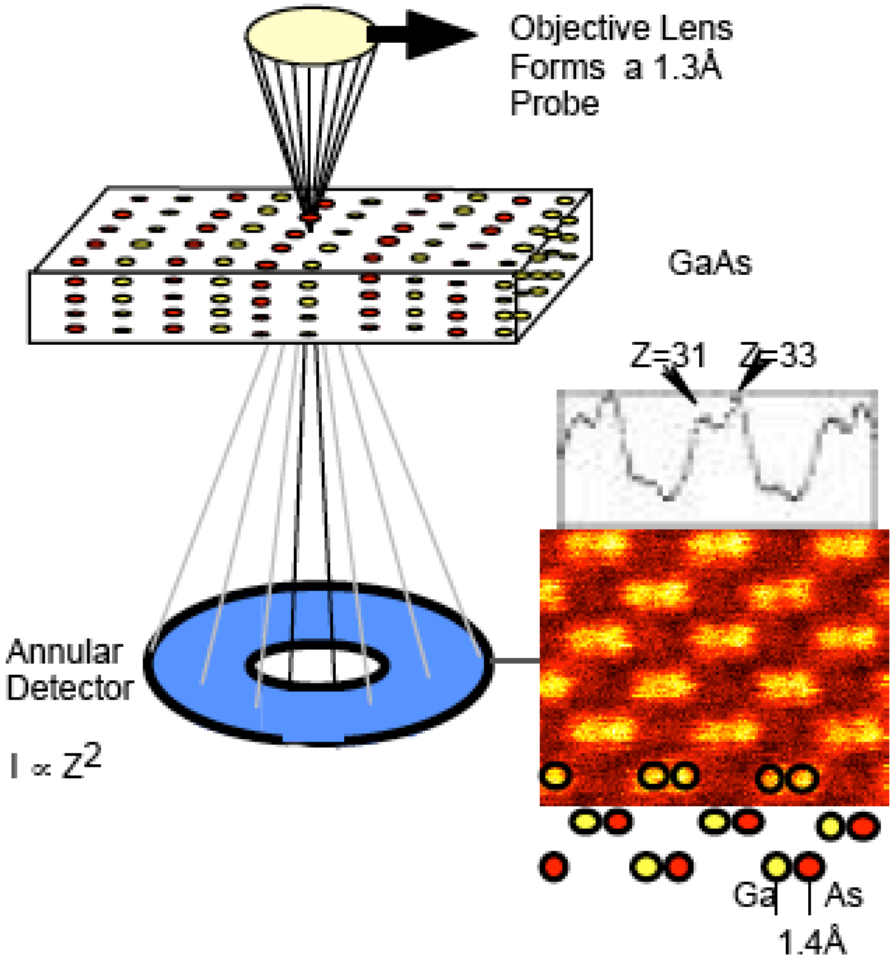


Here the electron beam is rastered across the sample in the *x*,*y* plane and the scattering is recorded on a detector.

Depending on the size and type of the detector two different kinds of STEM can be performed:

Small detector = standard STEM

* bright-field

Large annular detector = *Z* contrast

* dark-field

# Scanning transmission electron microscopy (STEM)

STEM is highly sensitive to the atomic number, especially high-angle STEM, known as high-angle annular dark-field (HAADF) or *Z*-contrast.

Right is an image of antimony in silicon, where the Sb atoms are easily seen as high intensity spots in the image.

For the case of Pu-bearing materials, such as $PuCoGa_5$, one could track where the Pu atoms diffuse as a function of time, i.e., as a function of self-irradiation damage.

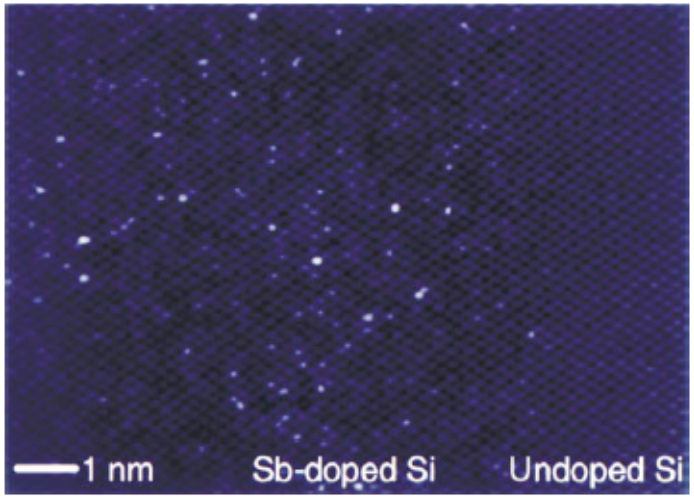


**Figure 1** Annular dark-field scanning transmission electron microscopy image of a cross-section of highly Sb-doped Si. The brightest dots (left) are atomic columns containing one or more Sb atoms, absent in substrate (right), where there is no Sb. Thickness variations along the wedge have been subtracted using a second-order polynomial fit. The image has been low-pass filtered to remove scan noise, and is displayed with a nonlinear intensity scale to highlight bright features.

(Voyles *et al.* Nature 2002).

# Convergent-beam electron diffraction (CBED)

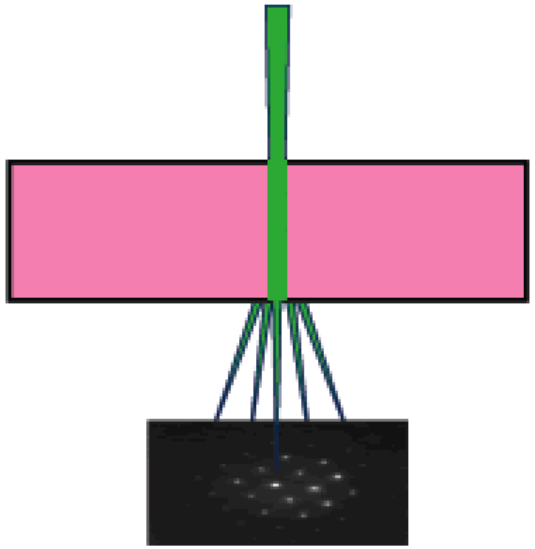

Normal electron diffraction is formed with parallel illumination of the electron beam so that Bragg reflections are spots

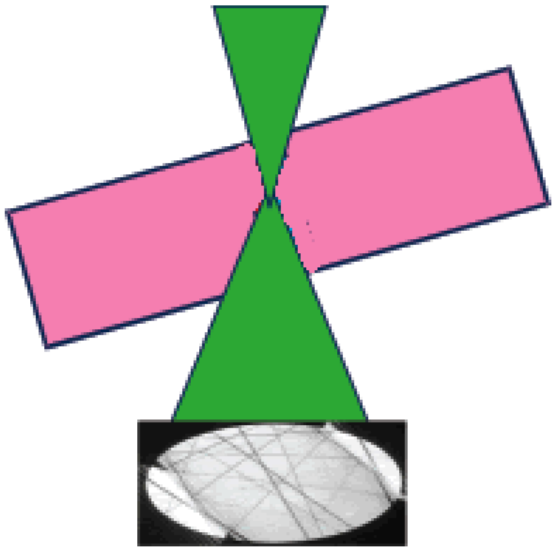

In CBED the electron beam is convergent, so that the reflections are disks rather than spots.

Zone axis CBED pattern

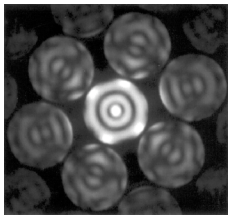

Two- or three-beam condition

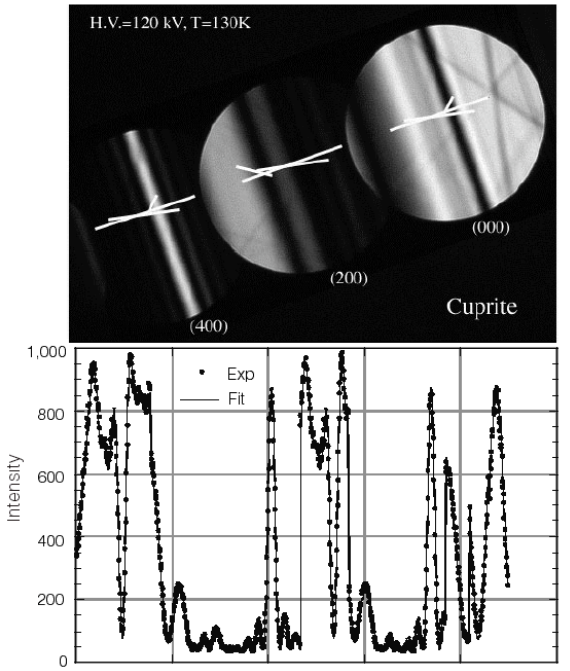

# 3D real space charge density

CBED disks may be used to extract the charge density of a given material, such as the copper oxide seen right.

Experimental charge density mapping has been performed for *s*-, *p*- and *d*-electron materials, but not yet for *f*-electron materials.

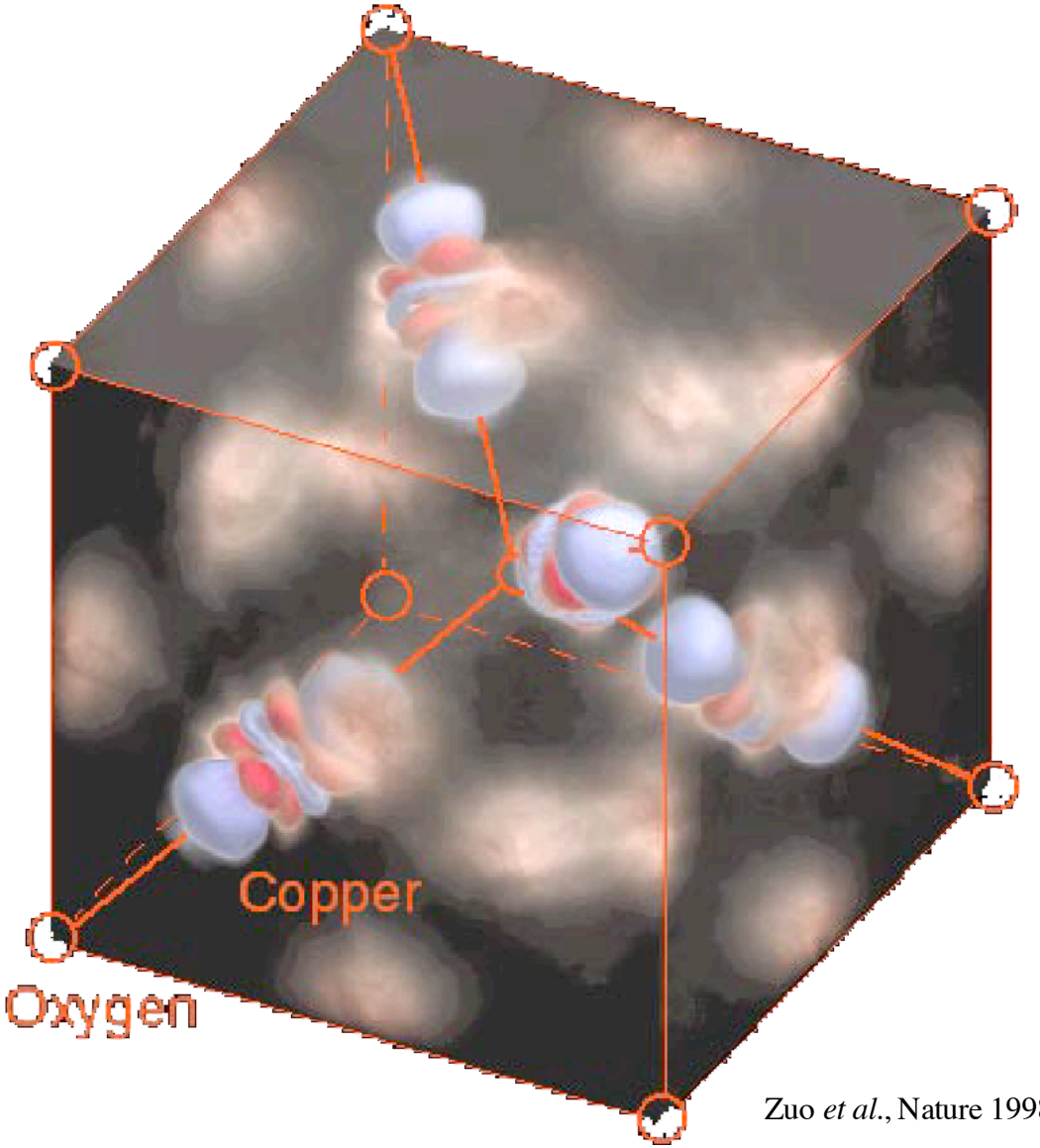


Zuo *et al.*, Nature 1998

# Electron scattering

**Elastic → Structure**

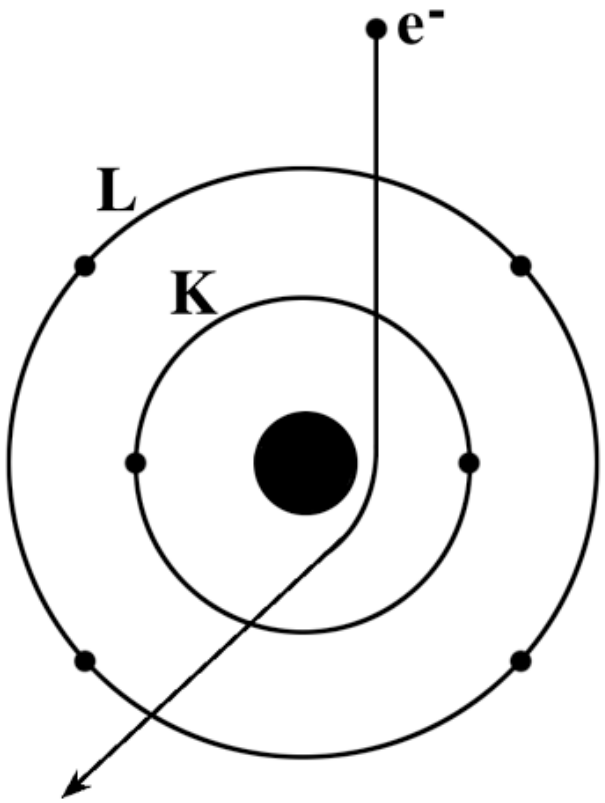


**Inelastic → Chemistry**

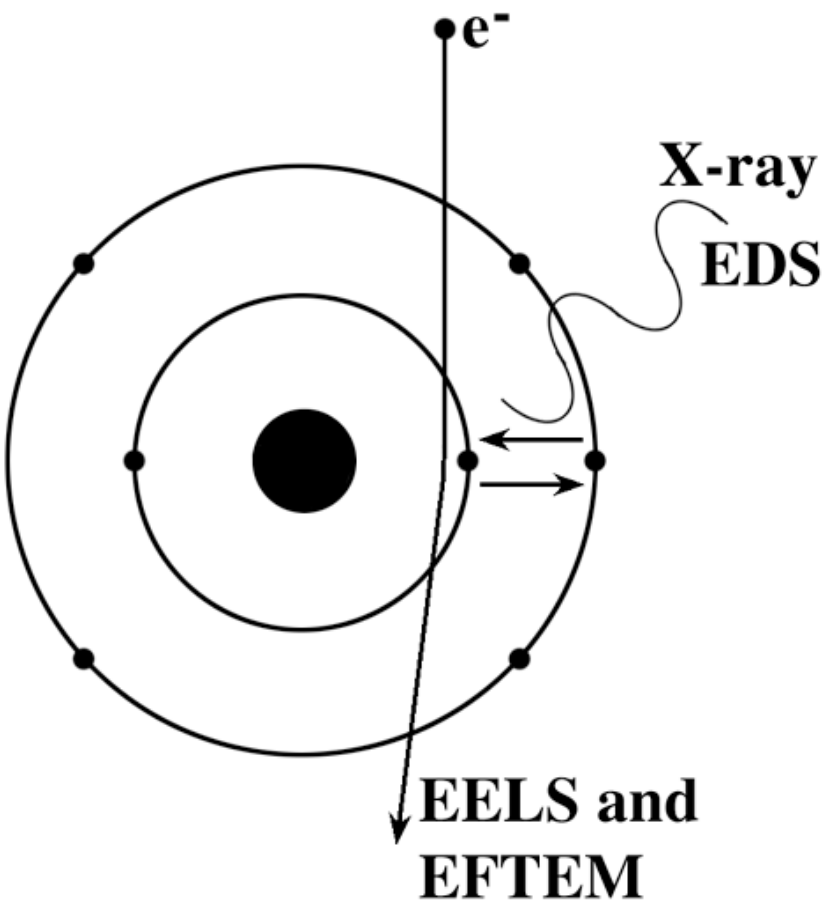

# Energy dispersive X-ray spectroscopy

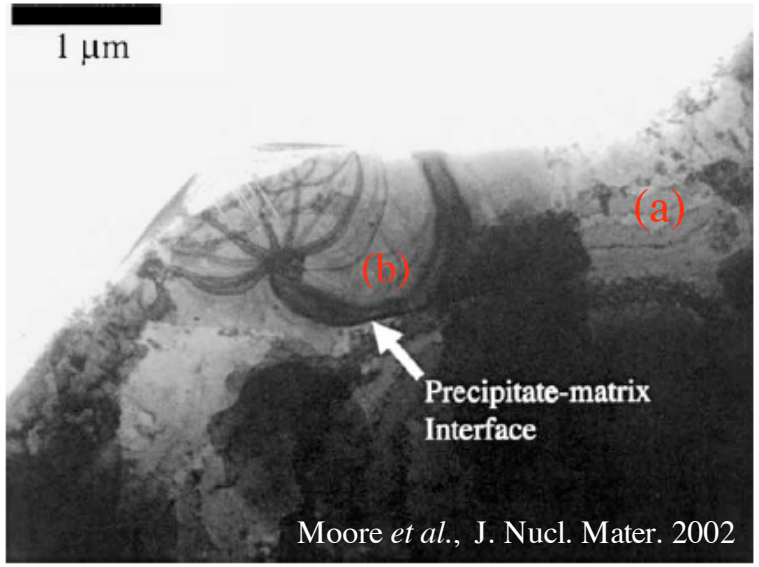


Fig. 2. A bright-field TEM image of one of the ζ $Pu_6Fe$ precipitates contained in a fcc Pu matrix. The precipitate–matrix interface is marked with an arrow.

EDXS spectra help identify $Pu_6Fe$.

Chemical analysis shows:
1) Ga in the δ matrix.
2) Fe and Ni in the $Pu_6Fe$.

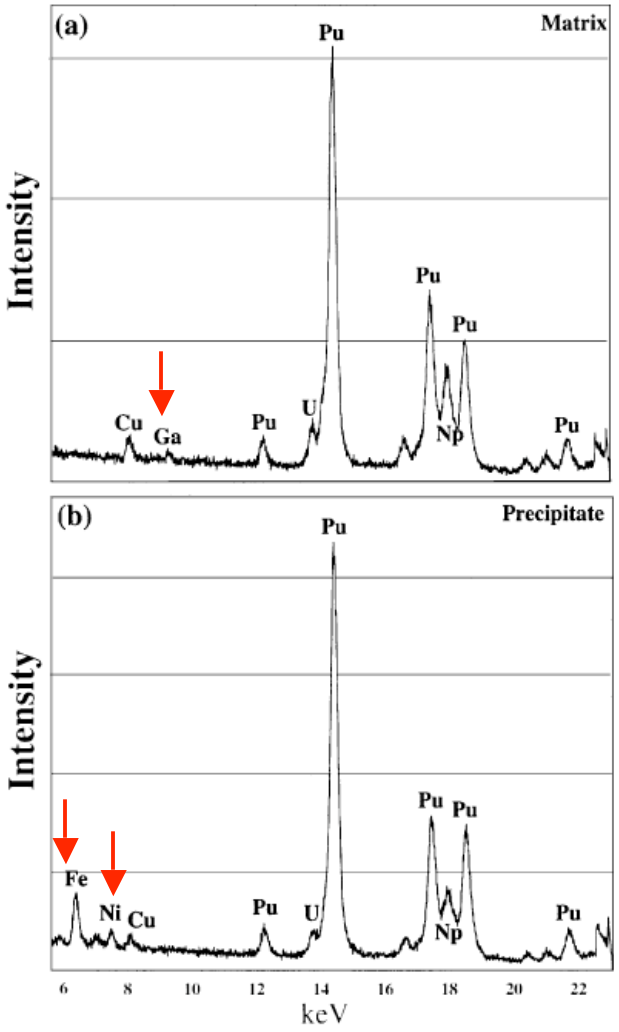


Fig. 3. Two EDXS spectra taken from; (a) the fcc Pu matrix and (b) one of the ζ $Pu_6Fe$ precipitates. Notice that an Fe peak is found in the spectrum for ζ $Pu_6Fe$, but is absent in the spectrum for the Pu matrix.

# Energy dispersive X-ray spectroscopy

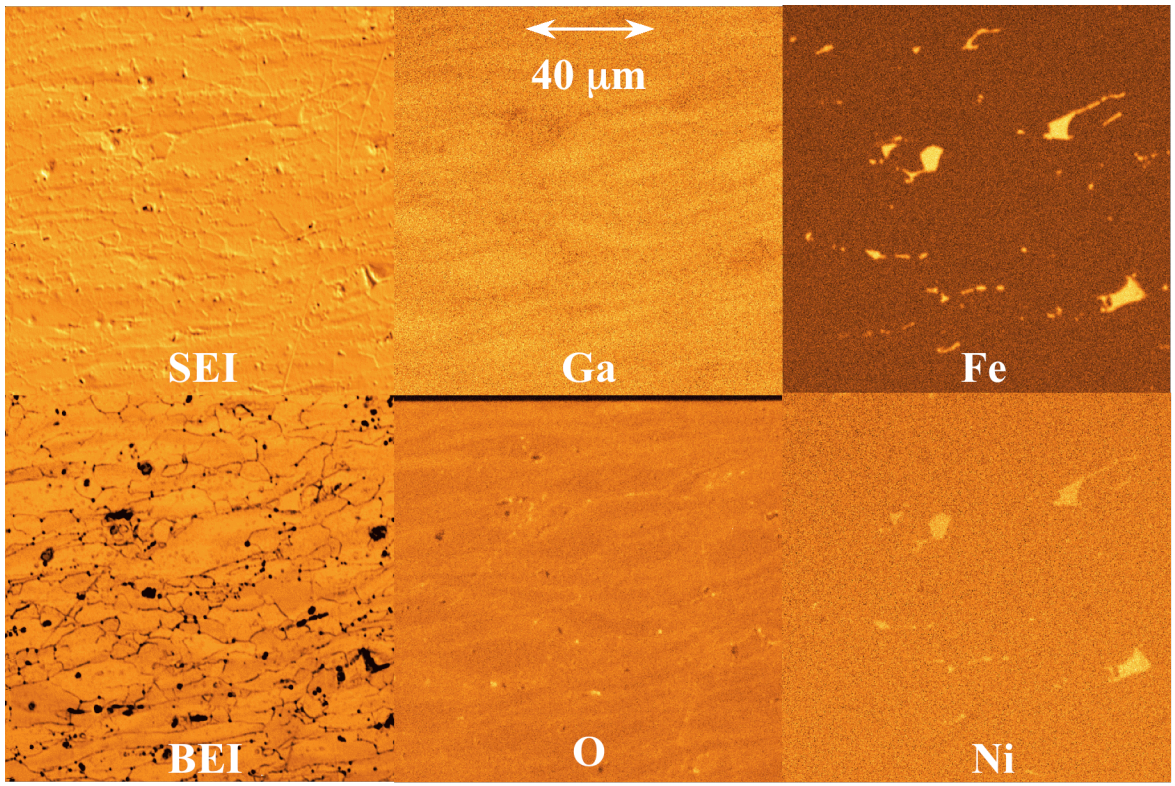


EDXS spectra can be used to make a 2D compositional map by rastering the beam across the specimen.

In this case we used a scanning electron microscope (SEM) on a Pu-Ga alloy.

The images show: Ga is uniform in the δ matrix, small amounts of O, and Fe and Ni in the same areas, likely as $Pu_6Fe$.

# Electron energy-loss spectroscopy

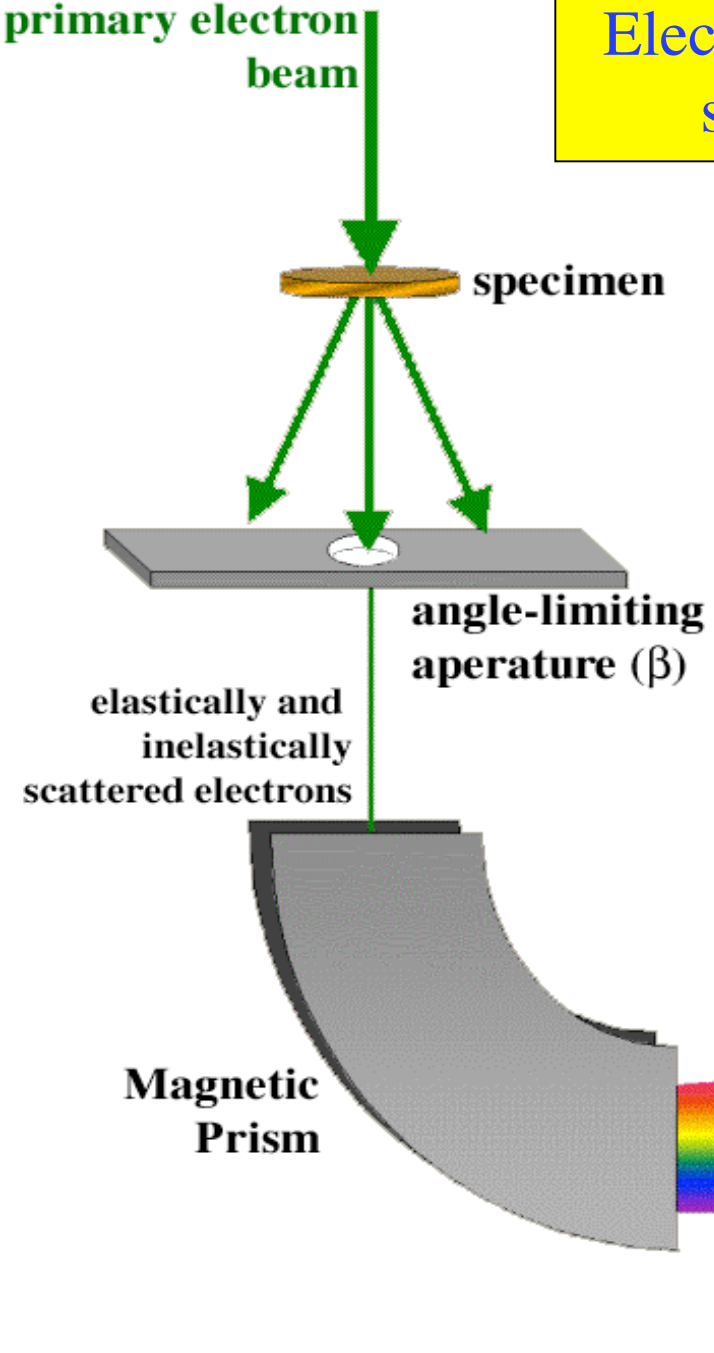


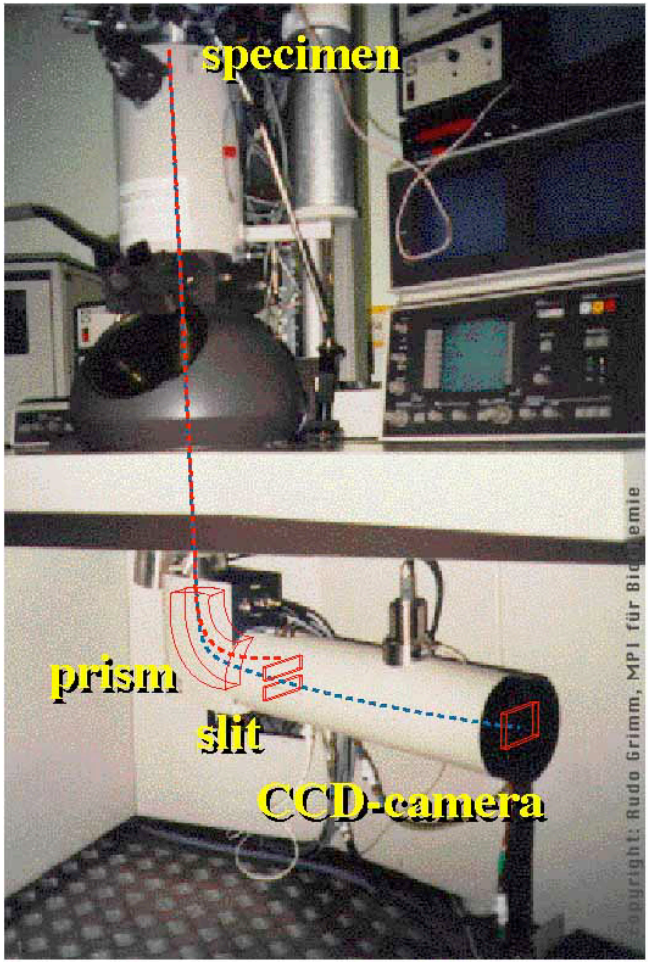

# Electron energy-loss spectroscopy

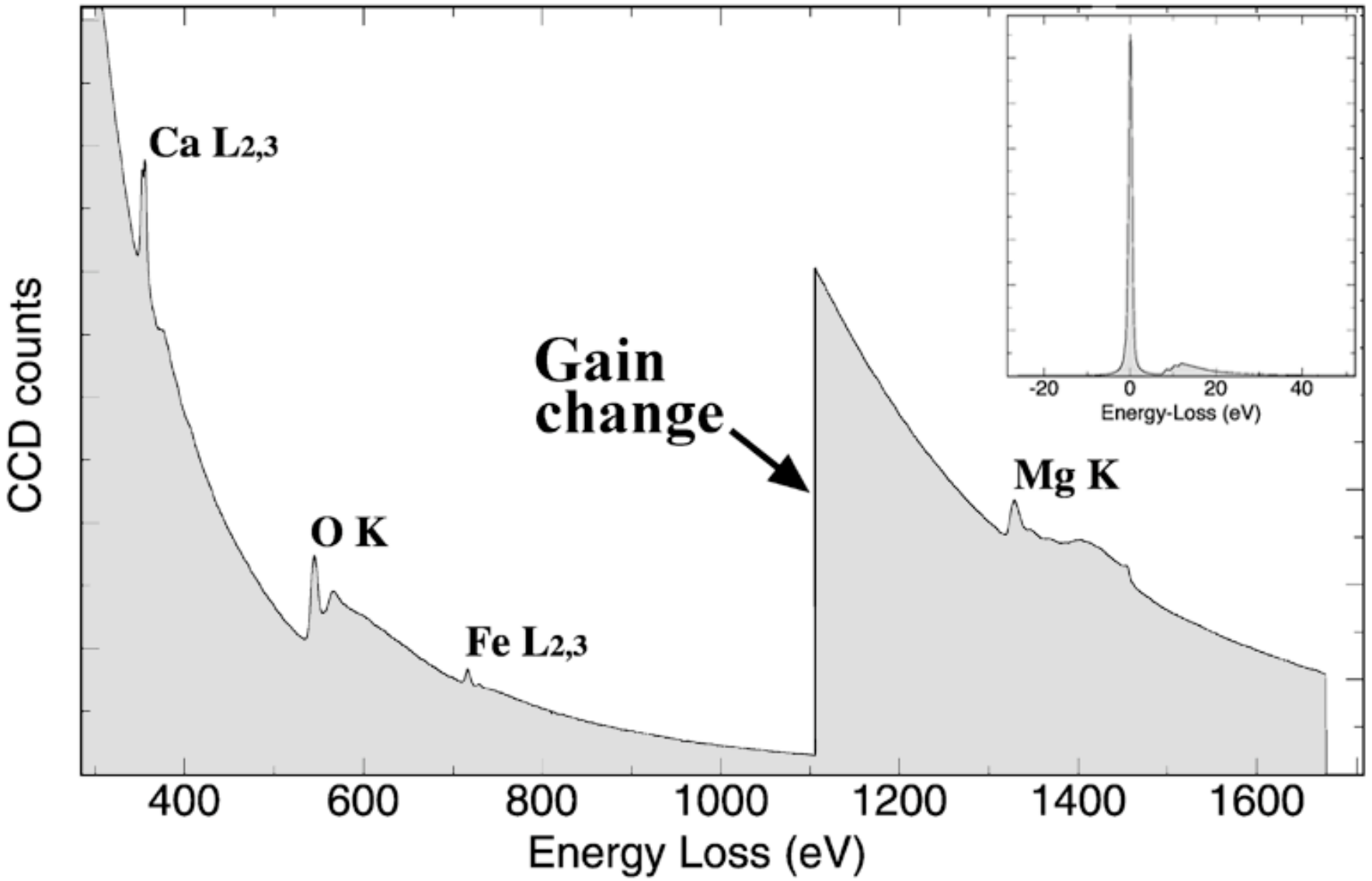

# Using EELS ionization edges to extract physics: The branching ratio of $d \rightarrow f$ transitions

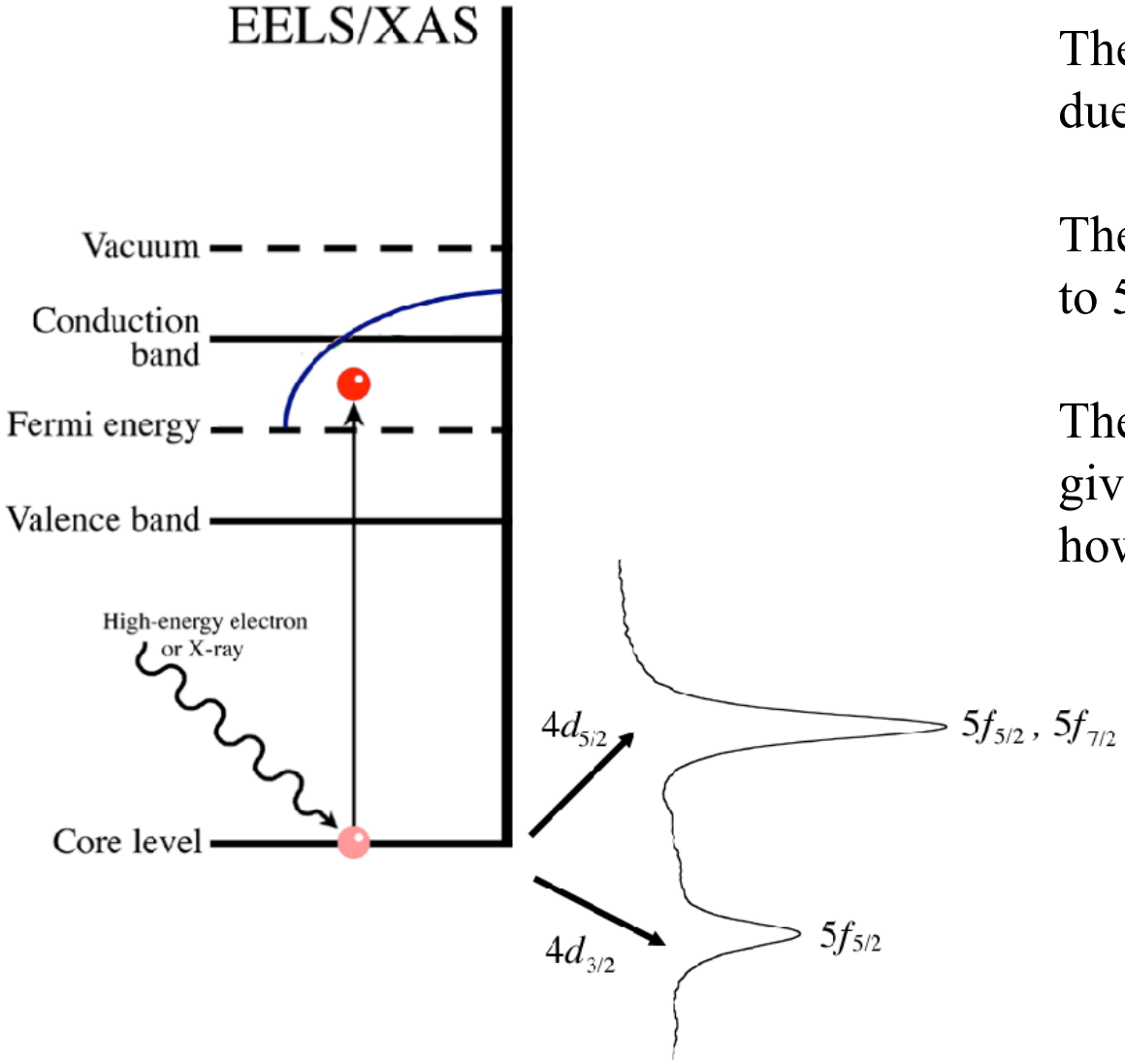


The branching ratio emanates due to dipole selection rules.

The core 4*d* states are excited to 5*f* final states.

The intensity in each peak gives us information about how the 5*f* states are occupied.

# Extracting the branching ratio from EELS spectra

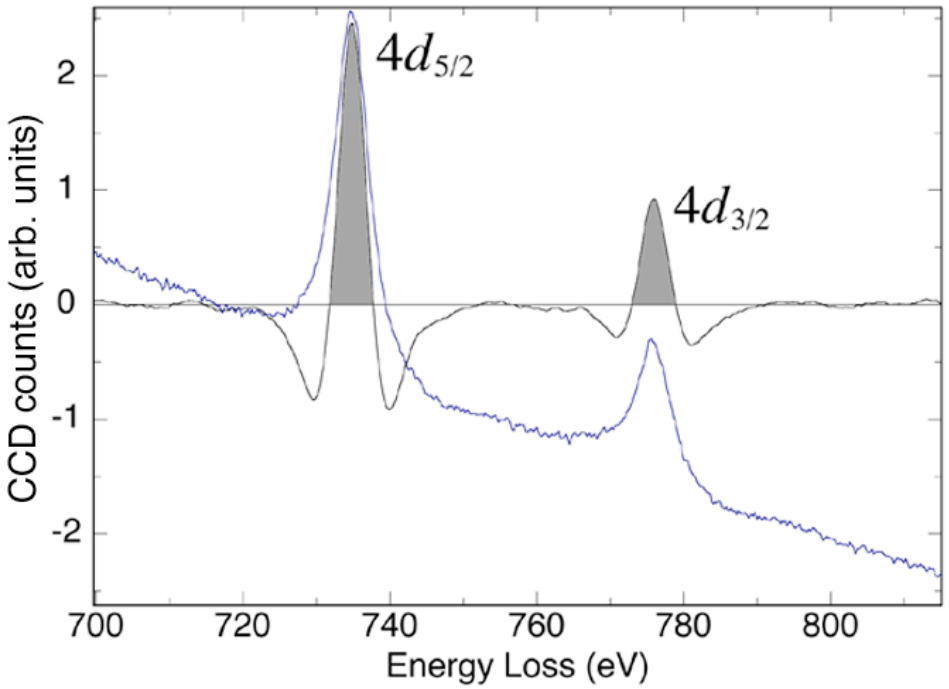


The branching ratio $B$ is defined as:

$$B = \frac{A_{5/2}}{\left[A_{5/2} + A_{3/2}\right]}$$

where $A_{5/2}$ and $A_{3/2}$ are the areas under the $N_5$ and $N_4$ peaks, respectively, in the EELS spectra.

In order to extract the peak areas $A_{5/2}$ and $A_{3/2}$ we take the second derivative (black line) of the raw spectra (blue line) and integrate above the zero, which is the gray areas in the plot above.

This has proven to be a very precise way of measuring the peak areas in our EELS spectra without the need of a background removal procedure.

# Extracting physics about actinide materials from the branching ratio of EELS spectra

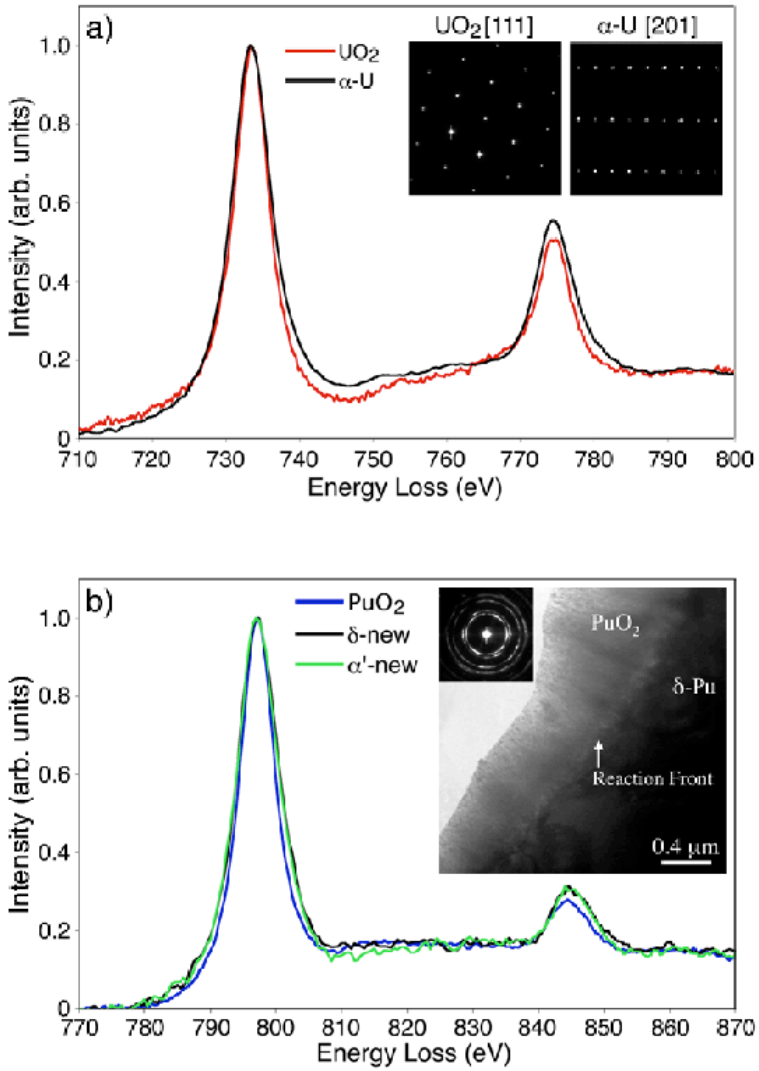


Moore *et al.* PRB 73 2006.

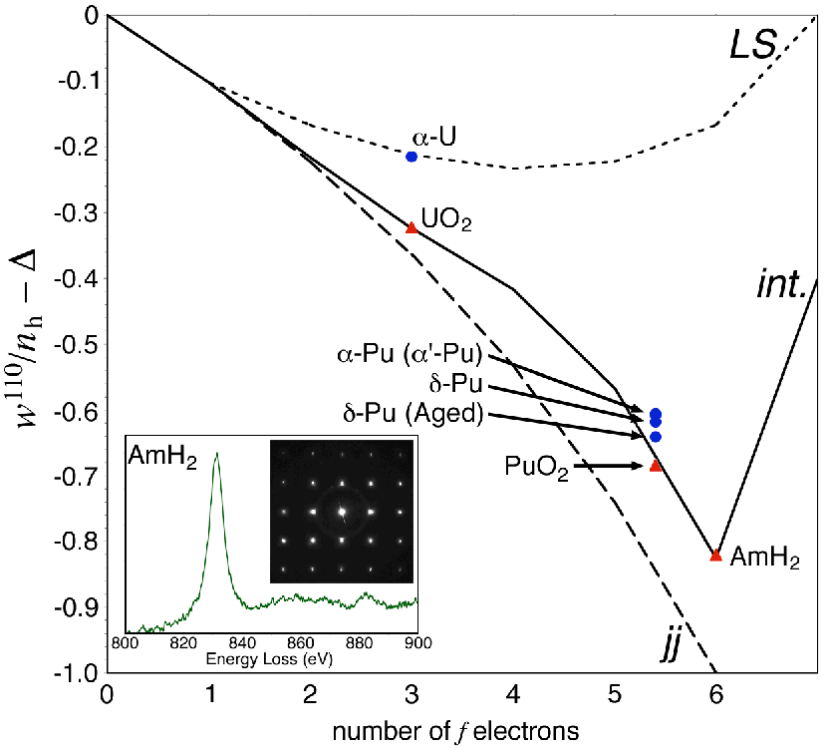


Using the experimental branching ratios, many-electron atomic spectral simulations, and sum rules we may extract the electron occupation of the $j$ = 5/2 and 7/2 sublevels of the 5f states, and thus the angular momentum coupling scheme for each actinide material.

# Energy-filtered transmission electron microscopy (EFTEM)

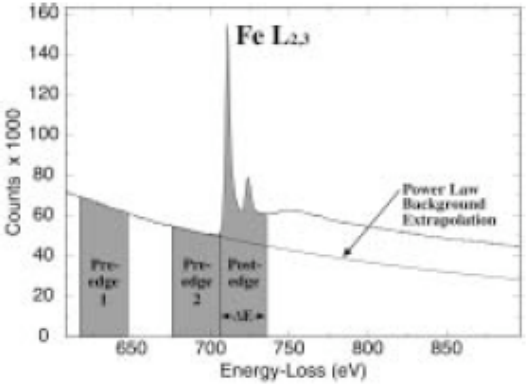


FIGURE 1. An EELS spectrum showing the placement of energy windows (ΔE) used for the acquisition of pre-edge and post-edge images. These energy-filtered images are then used to create jump-ratio images and elemental maps.

Using the area of an EELS spectra near an ionization edge 2D chemical maps can be formed.

The Fe edge above was used to form the images right of an Fe-bearing chain-silicate called a pyroxene.

* two window = qualitative
* three window = quantitative

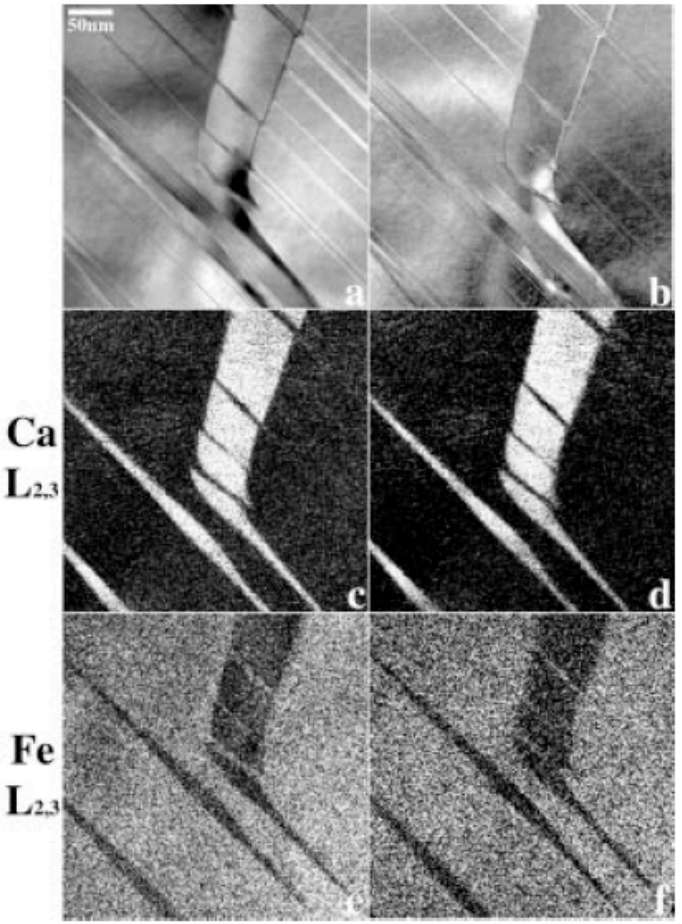


FIGURE 10. A series of EFTEM images acquired from the central region of Figure 9. (a) zero-loss, (b) thickness map, (c) Ca $L_{2,3}$ jump-ratio image, (d) Ca $L_{2,3}$ elemental map, (e) Fe $L_{2,3}$ jump-ratio image, and (f) Fe $L_{2,3}$ elemental map. The thickness map shows that the area analyzed is quite uniform in thickness (ignoring residual diffraction contrast).

Moore *et al. American Mineralogist* 86 (7-8) 2001.

# Energy-filtered transmission electron microscopy (EFTEM)

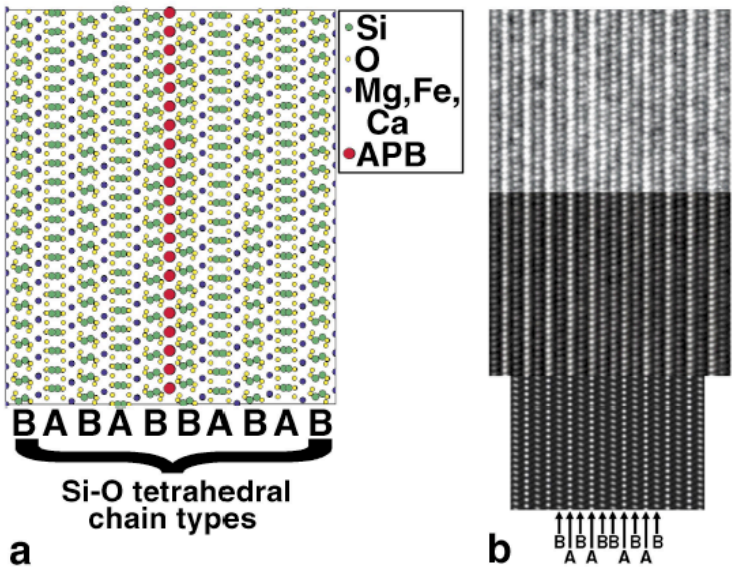


FIGURE 3. (a) A [010] projection of the pigeonite structure containing a (100) APB used for HRTEM simulations. (b) An experimental HRTEM image acquired parallel to the [010] zone axis (top), the same experimental image with a background filter applied to reduce noise (middle), and a simulated image with a sample thickness T = 10 nm and an objective lens defocus $\Delta f = -54$ nm (bottom). In pigeonite there are two symmetrically distinct Si-O tetrahedral chains, each with a different degree and sense of rotation. Therefore, when viewed on the [010] zone axis, there are (100) layers that consist of A chains and (100) layers that consist of B chains. Augite, on the other hand, has symmetrically equivalent chains. When viewed parallel to [010], there is an axis of twofold rotation passing through the M sites and the Si-O tetrahedral chains are the same. Note that the local atomic structure of the APB in (a) is similar to that of augite. HRTEM simulations with more than 50% Ca at the APB were not performed. This is because in the [010] projection, an APB contains 1/2M1 and 1/2M2 cation sites. The M1 sites do not readily accept Ca and, therefore, Ca occupancies greater than 50% are not energetically favorable.

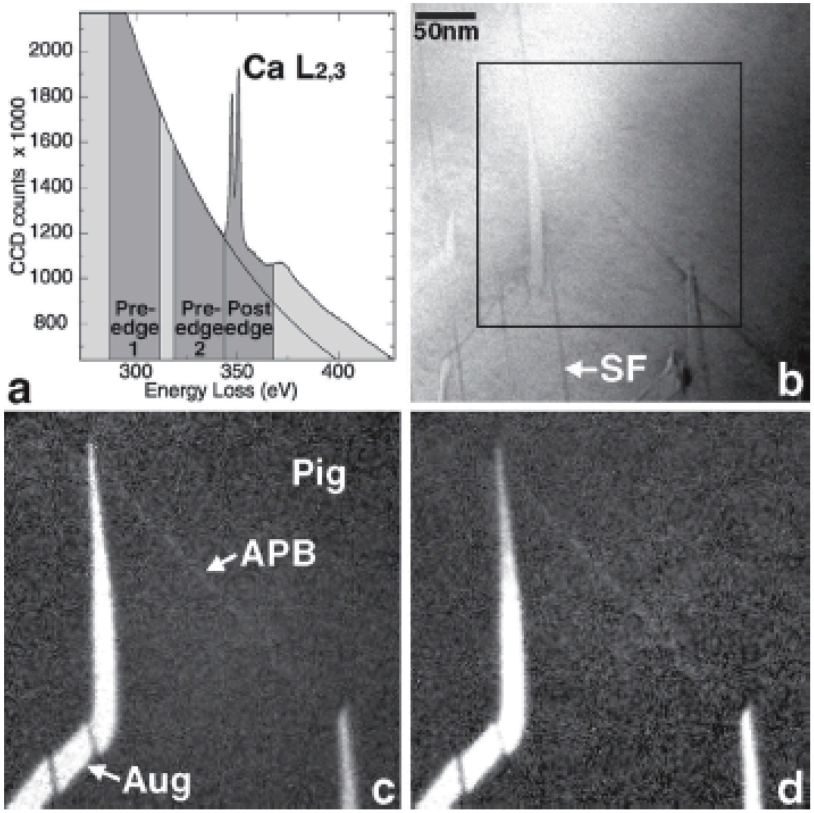


Moore *et al. American Mineralogist* 86 (10) 2001.

EFTEM can be performed at or near atomic resolution as shown above for the anti-phase boundary (APB) in the same chain-silicates.

In this case the Ca $L_{2,3}$ edge was used to form images showing segregation at the APB.

# *In situ* heating and cooling capabilities

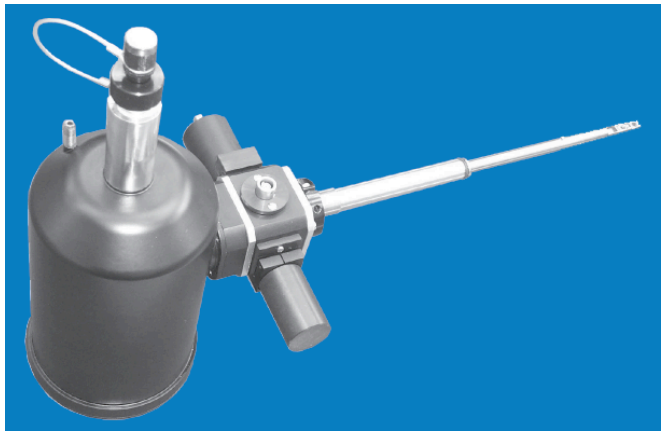

We have a suite of vacuum-transfer holder for the TEM that can perform heating and cooling experiments in the microscope.

Heating: can achieve 800°C for extended periods of time.

Presently hot-stage experiments are being performed on Pu-Ga alloys to examine He bubble growth, diffusion, and coalescence.

Cooling: A new liquid-He holder has achieved 8°K for 45 minutes of working time in the TEM.

Give real time observations of how self-induced radiation damage affects the lattice.